# Radiative lepton model in a non-invertible fusion rule

Takaaki Nomura,<sup>1,\*</sup> Hiroshi Okada,<sup>2,†</sup> and Yoshihiro Shigekami<sup>2,‡</sup>

<sup>1</sup>College of Physics, Sichuan University, Chengdu 610065, China

<sup>2</sup>Department of Physics, Henan Normal University, Xinxiang 453007, China

(Dated: October 21, 2025)

We propose a radiatively induced lepton mass model introducing a  $Z_2$  gauging  $Z_5$  fusion rule. In our framework, the charged-lepton mass matrix is generated at one loop level via dynamical breaking of the fusion rule. On the other hand, the neutrino mass matrix is induced at one-loop level without breaking the fusion rule. As a direct consequence of the loop induced charged lepton masses, we can also consider lepton flavor violations, electron and muon g-2, and charged-lepton electric dipole moments that come into our valid phenomenological discussion. Then, we perform numerical analysis and show some interesting tendency on Dirac CP phase, two Majorana phases, charged-lepton electric dipole moments and the neutrinoless double beta decay, all of which depends on their arguments where we fix the absolute values of our free parameters in order to satisfy experimental data of the lepton masses and mixing angles.

PACS numbers:

<sup>\*</sup>Electronic address: nomura@scu.edu.cn

<sup>†</sup>Electronic address: hiroshi3okada@htu.edu.cn ‡Electronic address: shigekami@htu.edu.cn

#### I. INTRODUCTION

The radiative seesaw model is one of the attractive scenarios to understand a mechanism of minuscule masses such as active neutrinos and electron at low energy scale beyond the standard model (BSM). In addition, we can potentially discuss plenty of phenomenology such as lepton flavor violations (LFVs), electron/muon anomalous magnetic dipole moments (electron/muon q-2), charged-lepton electric dipole moments (EDMs), and dark matter (DM), all of which can be connected to such tiny mass particles inside the loop. To obtain relevant terms in order to induce loop diagrams as leading contributions, non-invertible fusion rules are recently applied to these kinds of models. These selection rules possess some intriguing nature. The first remarkable nature is that the rules can forbid undesired terms at tree level but violate at loop level in a dynamical manner. The second one is that these rules provide an exact symmetry such as  $Z_2$  that never be broken at any orders and play a role in stabilizing the DM candidate. The third one is that they give some mass textures to reduce mass parameters in quark and lepton sectors, and possibly lead to predictions <sup>1</sup>. Note here that the second and third nature can be replaced by the other symmetries such as discrete flavor symmetries [23–26]. However, the first one is totally unique for the case of non-invertible fusion rule. These nature would pave the way for constructing new models and it is worth for exploring applications of the rule.

In this work, we apply  $Z_2$  gauging  $Z_5$  fusion rule  $\mathbf{Z}_5^{\mathbf{NI}}$ , which consists of three elements  $\{\mathbb{I}, a, b\}$ , where all are supposed to be real and commutable each other; backgrounds and rules for  $Z_2$  gauging  $Z_N$  symmetry can be referred to refs. [9, 10]. For these elements, we have

$$a \otimes a = \mathbb{I} \oplus b, \quad a \otimes b = a \oplus b, \quad b \otimes b = \mathbb{I} \oplus a, \quad \mathbb{I} \otimes (\mathbb{I}, a, b) = (\mathbb{I}, a, b).$$
 (1)

For a radiative lepton mass model, we introduce left- and right-handed Majorana fermions, isospin doublet inert boson  $\eta$ , singly charged-boson  $S^{-2}$ . We make use of the first and second nature in the  $\mathbf{Z}_{5}^{\mathbf{NI}}$  fusion rules. Therefore, the charged-lepton mass matrix can be induced at one-loop via dynamical breaking of  $\mathbf{Z}_{5}^{\mathbf{NI}}$ . On the other hand, the neutrino mass matrix is generated at one-loop level where  $\mathbf{Z}_{5}^{\mathbf{NI}}$  provides an accidental  $Z_{2}$  symmetry that never be broken at any order. This is the same as the case of Ma model [27]. In addition, through the charged-lepton sector, we can also

<sup>&</sup>lt;sup>1</sup> See the following refs. [1–22], in which authors proposed several ways to apply these rules for phenomenology.

<sup>&</sup>lt;sup>2</sup> We can also realize the same interactions by applying Fibonacci fusion rules that is the minimum fusion ones. However, this scenario induces terms that are forbidden at tree level, by radiative corrections. Some of these radiative corrections include infinity that never be able to be canceled out. We thus do not adopt the minimal Fibonacci fusion rules to keep predictability of the model. We briefly show some more detail in the model part.

|                     | $L_L$          | $\ell_R$ | $N_L$ | $N_R$ | H             | η             | $S^-$ |
|---------------------|----------------|----------|-------|-------|---------------|---------------|-------|
| $SU(2)_L$           | 2              | 1        | 1     | 1     | 2             | 2             | 1     |
| $U(1)_Y$            | $-\frac{1}{2}$ | -1       | 0     | 0     | $\frac{1}{2}$ | $\frac{1}{2}$ | -1    |
| $\mathbf{Z_5^{NI}}$ | b              | a        | a     | a     | I             | b             | b     |

TABLE I: Charge assignments of relevant fermions and bosons under  $SU(2)_L \otimes U(1)_Y \otimes \mathbf{Z_5^{NI}}$ . All fermions have to have three generations, and all new particles are singlet under  $SU(3)_c$ .

discuss LFVs, electron/muon g-2 and charged-lepton EDMs <sup>3</sup>.

This paper is organized as follows. In section II, we review our lepton seesaw model and explain how to induce the small charged-lepton masses as well as the neutrino masses. We also discuss several phenomenology related to the charged-leptons. In section III, we demonstrate several numerical  $\chi^2$  results satisfying neutrino observables, LFVs, electron/muon g-2, and charged-lepton EDMs in cases of normal and inverted hierarchies. In section IV, we summarize and conclude.

### II. MODEL SETUP

Here, we review our model setup in which we introduce  $Z_2$  gauging  $Z_5$  fusion rule  $\mathbf{Z}_5^{\mathbf{NI}}$ . Firstly the lepton masses at tree-level are forbidden by assigning  $\mathbf{Z}_5^{\mathbf{NI}}$  charge to lepton particles. Then, in order to generate the lepton mass matrix at one-loop level, we introduce three families of left/right neutral Majorana fermions  $N_{L/R}$ , an isospin doublet inert boson  $\eta \equiv [\eta^+, (\eta_R + i\eta_I)/\sqrt{2}]^T$  and an isospin singlet singly-charged-boson  $S^-$  in addition to the SM particles. Moreover,  $\eta$  and  $S^-$  do not acquire non-zero vacuum expectation values (VEVs). Note here that the charged-lepton mass matrix is generated by dynamically breaking of this symmetry, and LFVs, g-2, and EDMs have the same origin as the charged-lepton mass matrix [28–30]. On the other hand the neutrino mass matrix is obtained without violating the fusion rule, as we will show later. The particle contents and their charge assignments are summarized in Table I.

Under the symmetry, the renomalizable Lagrangian is given by

$$-\mathcal{L}_{\ell} = y_{ii}^{\ell} \overline{L_{L_{i}}} \eta \ell_{R_{i}} + f_{ia}^{R} \overline{L_{L_{i}}} \tilde{\eta} N_{R_{a}} + f_{ia}^{L} \overline{L_{L_{i}}} \tilde{\eta} N_{L_{a}}^{C} + g_{ai}^{R} \overline{N_{R_{a}}^{C}} \ell_{R_{i}} S^{+} + g_{ai}^{L} \overline{N_{L_{a}}} \ell_{R_{i}} S^{+}$$

$$+ (M_{D})_{aa} \overline{N_{L_{a}}} N_{R_{a}} + (M_{R})_{ab} \overline{N_{R_{a}}^{C}} N_{R_{b}} + (M_{L})_{ab} \overline{N_{L_{a}}} N_{L_{b}}^{C} + \text{h.c.},$$

$$(2)$$

where  $\tilde{\eta} \equiv i\tau_2\eta^*$  being  $\tau_2$  the second Pauli matrix.  $y^{\ell}$  and  $M_D$  can be diagonal matrices without

<sup>&</sup>lt;sup>3</sup> Even though we can discuss the nature of DM candidate, we focus on the other phenomenology such as EDMs in this paper.

loss of generality. The Higgs potential is given by

$$\mathcal{V} = -\mu_H^2 |H|^2 - \mu_\eta^2 |\eta|^2 - \mu_S^2 |S^-|^2 + \mu_0 \left( H^T (i\tau_2) \eta S^- + \text{h.c.} \right) 
+ \lambda_H |H|^4 + \lambda_\eta |\eta|^2 + \lambda_S |S^-|^4 + \lambda_{H\eta} |H|^2 |\eta|^2 + \lambda'_{H\eta} |H^{\dagger} \eta|^2 + \lambda''_{H\eta} \left( (H^{\dagger} \eta)^2 + \text{h.c.} \right) 
+ \lambda_{HS} |H|^2 |S^-|^2 + \lambda_{\eta S} |\eta|^2 |S^-|^2.$$
(3)

Especially,  $\lambda''_{H\eta}$  term contributes to generating the neutrino mass matrix at one-loop level, and  $\mu_0$  term contributes to the radiative charged-lepton mass matrix.

Before moving to see radiative mass generation for each fermion sector, we comment on the physical phases of the model. In the Higgs potential in Eq. (3), there are two possible complex parameters,  $\mu_0$  and  $\lambda''_{H\eta}$ . These phases can be absorbed into the two phases of H,  $\eta$  and  $S^{\pm}$ . Since other parameters in the Higgs potential are real by definition, there is no physical CP source from the potential. In the Lagrangian in Eq. (2), on the other hand, we have lots of complex parameters. It is clear that all these phases cannot be removed by considering phase redefinition for remaining fields. As a results, we truly have physical CP sources which result in non-zero (and non-trivial) predictions for charged-lepton EDMs. For example, following phases are invariant under any rephasing for fields:

$$\theta_{\text{phys}} = \arg \left[ \frac{f_{ia}^R g_{ia}^L}{f_{ia}^L g_{ia}^R} \right], \ \arg \left[ \frac{(M_D)_{aa}^2}{(M_R)_{aa}(M_L)_{aa}} \right], \ \cdots, \tag{4}$$

with no summation for i, a.

Notice that if we use the Fibonacci rules,  $1 \otimes \tau = \tau$  and  $\tau \otimes \tau = 1 \oplus \tau$ , assigning  $\tau$  to  $\eta$  and  $S^-$ , we can write term  $(H^{\dagger}\eta)(\eta^{\dagger}\eta)$ . This term can induce terms such as  $(H^{\dagger}\eta)(H^{\dagger}H)$  and  $\eta^{\dagger}H$  through radiative correction. Those radiative corrections would induce divergence which could not be eliminated as the tree level coupling is absent. In addition,  $\eta^{\dagger}H$  term spoils inert nature of  $\eta$  and the mechanism of the model does not work. Therefore we need  $\mathbf{Z}_5^{\mathbf{NI}}$  as a relevant minimal selection rules where  $(H^{\dagger}\eta)(\eta^{\dagger}\eta)$  is forbidden as  $b \otimes b \otimes b$  does not contain  $\mathbb{I}$ .

## A. Neutral fermion mass matrix

The mass matrix of neutral fermion is induced via the second line of Lagrangian in Eq. (2), and its form is given by

$$\left(\begin{array}{cc}
\overline{N_R^C} & \overline{N_L}
\end{array}\right) \begin{pmatrix} M_R & M_D \\
M_D & M_L
\end{pmatrix} \begin{pmatrix} N_R \\
N_L^C
\end{pmatrix} \equiv \left(\begin{array}{cc}
\overline{N_R^C} & \overline{N_L}
\end{array}\right) M_N \begin{pmatrix} N_R \\
N_L^C
\end{pmatrix},$$
(5)

where we omit generation indices, and each block is understood as  $3 \times 3$  matrix.  $M_N$  is then understood as a  $6 \times 6$  symmetric matrix. Note that due to our assumption about absence of VEVs for  $\{\eta, S^-\}$ , neutrinos do not mix with  $N_{L,R}$ . In order to diagonalize the above mass matrix, we suppose

$$M_R, M_L \ll M_D, \tag{6}$$

which is an appropriate hypothesis when we consider the 't Hooft sense. Then, we first transform  $M_N$  as follows:

$$M_{N}' \equiv V_{N}^{(1)T} M_{N} V_{N}^{(1)} \equiv \begin{pmatrix} \frac{1}{\sqrt{2}} & \frac{1}{\sqrt{2}} \\ -\frac{1}{\sqrt{2}} & \frac{1}{\sqrt{2}} \end{pmatrix} \begin{pmatrix} M_{R} & M_{D} \\ M_{D} & M_{L} \end{pmatrix} \begin{pmatrix} \frac{1}{\sqrt{2}} & -\frac{1}{\sqrt{2}} \\ \frac{1}{\sqrt{2}} & \frac{1}{\sqrt{2}} \end{pmatrix}$$

$$= \begin{pmatrix} M_{D} + \frac{M_{L} + M_{R}}{2} & \frac{M_{L} - M_{R}}{2} \\ \frac{M_{L} - M_{R}}{2} & -M_{D} + \frac{M_{L} + M_{R}}{2} \end{pmatrix} \equiv \begin{pmatrix} M_{D} + m_{+} & m_{-} \\ m_{-} & -M_{D} + m_{+} \end{pmatrix},$$
(7)

where  $m_- \lesssim m_+ \ll M_D$ .  $M_N'$  is then block-diagonalized as follows:

$$(\Omega P)^T M_N'(\Omega P) = \begin{pmatrix} M_D - m_+ & \mathbf{0} \\ \mathbf{0} & M_D + m_+ \end{pmatrix} \equiv M_N'', \tag{8}$$

$$\Omega PU_N = \begin{pmatrix} \mathbf{1} & -\frac{1}{2}M_D^{-1}m_- \\ \frac{1}{2}m_-^{\dagger}M_D^{-1} & \mathbf{1} \end{pmatrix} \begin{pmatrix} \mathbf{0} & \mathbf{1} \\ i \cdot \mathbf{1} & \mathbf{0} \end{pmatrix}. \tag{9}$$

Here, bold number  $\mathbf{0}(\mathbf{1})$  represents  $3 \times 3$  zero (unit) matrix. Finally, the above mass matrix is diagonalized by

$$U_N^T M_N'' U_N = \begin{pmatrix} U_R^T & \mathbf{0} \\ \mathbf{0} & U_L^T \end{pmatrix} \begin{pmatrix} M_D - m_+ & \mathbf{0} \\ \mathbf{0} & M_D + m_+ \end{pmatrix} \begin{pmatrix} U_R & \mathbf{0} \\ \mathbf{0} & U_L \end{pmatrix} = \begin{pmatrix} D_R & \mathbf{0} \\ \mathbf{0} & D_L^C \end{pmatrix}. \tag{10}$$

 $M_N$  is approximately diagonalized via  $V_N \equiv V_N^{(1)} \Omega P U_N$  as  $V_M^T M_N V_N \sim \text{diag}(D_R, D_L^C)$ . Note that we have used an assumption that  $M_D$  should be proportional to the  $3 \times 3$  unit matrix in order to achieve our diagonalization [31, 32];

$$M_D \approx M_0 \times \mathbf{1}.\tag{11}$$

Then,  $M_D \pm m_+$  is given by

$$M_D \pm m_+ \simeq \begin{pmatrix} M_0 \pm \delta_{11} & \pm \delta_{12} & \pm \delta_{13} \\ \pm \delta_{12} & M_0 \pm \delta_{22} & \pm \delta_{23} \\ \pm \delta_{13} & \pm \delta_{23} & M_0 \pm \delta_{33} \end{pmatrix}.$$
 (12)

Since the diagonal elements are greater than all the off-diagonal elements,  $M_D \pm m_+$  is approximately diagonalized by the following mixing matrices:

$$U_{R(L)} \approx \begin{pmatrix} 1 & \epsilon_{12}^{R(L)} & \epsilon_{13}^{R(L)} \\ -\epsilon_{12}^{R(L)} & 1 & \epsilon_{23}^{R(L)} \\ -\epsilon_{13}^{R(L)} & -\epsilon_{23}^{R(L)} & 1 \end{pmatrix}, \quad \epsilon_{ij}^{R(L)} \approx -\frac{\delta_{ij}}{\delta_{ii} - \delta_{jj}}, \quad (i \neq j) . \tag{13}$$

Since  $\epsilon^{R(L)}$  is expected to be tiny, we suppose  $|\delta_{ij}| \ll |\delta_{ii}|$  for  $i \neq j$  with i/j = 1, 2, 3. As a result, we find mass eigenstates for  $N_{R,L}$  as

$$N_{R_a} \equiv \sum_{\alpha=1}^{6} (V_N)_{a\alpha} \psi_{R_\alpha}, \quad N_{L_a}^C \equiv \sum_{\alpha=1}^{6} (V_N)_{a+3,\alpha} \psi_{R_\alpha}. \tag{14}$$

Hereafter, mass eigenvalues for  $\psi_{R_{\alpha}}$  are indicated by  $D_{\alpha}$ .

## B. Charged-lepton mass matrix

The mass matrix of charged-leptons is induced at one-loop level via the following relevant Lagrangian:

$$f_{ia}^{R}\overline{L_{L_{i}}}\tilde{\eta}N_{R_{a}} + g_{bj}^{L}\overline{N_{L_{b}}}\ell_{R_{j}}S^{+} + f_{ia}^{L}\overline{L_{L_{i}}}\tilde{\eta}N_{L_{a}}^{C} + g_{bj}^{R}\overline{N_{R_{b}}^{C}}\ell_{R_{j}}S^{+} + \text{h.c.},$$

where  $\mu_0 H^T(i\tau_2)\eta S^-$  plays a role in connecting  $S^{\pm}$  and  $\eta^{\pm}$  to construct the one-loop diagram <sup>4</sup>. Then, these terms are rewritten in terms of mass eigenstates of  $N_{L,R}$  ( $\psi_{R_{\alpha}}$  in Eq. (14)) as follows (summation for a, b are implicitly understood):

$$\frac{f_{ia}^{R}(V_{N})_{a\alpha}}{\sqrt{2}}\overline{\ell_{L_{i}}}\eta^{-}\psi_{R_{\alpha}} + (V_{N}^{T})_{\alpha,b+3}g_{bj}^{L}\overline{\psi_{R_{\alpha}}^{C}}\ell_{R_{j}}S^{+} + \frac{f_{ia}^{L}(V_{N})_{a+3,\alpha}}{\sqrt{2}}\overline{\ell_{L_{i}}}\eta^{-}\psi_{R_{\alpha}} + (V_{N}^{T})_{\alpha,b}g_{bj}^{R}\overline{\psi_{R_{\alpha}}^{C}}\ell_{R_{j}}S^{+}$$

$$\equiv F_{i\alpha}\overline{\ell_{L_{i}}}\eta^{-}\psi_{R_{\alpha}} + G_{\alpha j}\overline{\psi_{R_{\alpha}}^{C}}\ell_{R_{j}}S^{+}, \tag{15}$$

where we define  $F_{i\alpha} \equiv \sum_{a=1}^{3} \left[ f_{ia}^{R}(V_{N})_{a\alpha} + f_{ia}^{L}(V_{N})_{a+3,\alpha} \right] / \sqrt{2}$  and  $G_{\alpha j} \equiv \sum_{b=1}^{3} \left[ (V_{N}^{T})_{\alpha,b+3} g_{bj}^{L} + (V_{N}^{T})_{\alpha,b} g_{bj}^{R} \right]$ . The resultant mass matrix for charged-lepton is given by

$$(m_{\ell})_{ij} = \frac{v_H \mu_0'}{\sqrt{2}(4\pi)^2 M_0} \frac{\tilde{F}_{i\alpha} \tilde{D}_{\alpha} \tilde{G}_{\alpha j}}{\tilde{D}_{\alpha}^2 - \tilde{m}_S^2} \left[ \frac{\tilde{D}_{\alpha}^2}{\tilde{D}_{\alpha}^2 - \tilde{m}_S^2} \ln \left( \frac{\tilde{D}_{\alpha}^2}{\tilde{m}_S^2} \right) + \frac{\tilde{D}_{\alpha}^2}{\tilde{D}_{\alpha}^2 - \tilde{m}_{\eta}^2} \ln \left( \frac{\tilde{D}_{\alpha}^2}{\tilde{m}_{\eta}^2} \right) \right], \tag{16}$$

where  $\mu'_0 \equiv f_{33}^R g_{33}^R \mu_0$ ,  $M_0$  is a typical scale of  $M_D$  (see Eq. (11)),  $\tilde{m}_{S,\eta} \equiv m_{S,\eta}/M_0$ ,  $\tilde{D}_{\alpha} \equiv D_{\alpha}/M_0$ ,  $\tilde{F} \equiv F/f_{33}^R$ , and  $\tilde{G} \equiv G/g_{33}^R$  with  $f_{33}^R$ ,  $g_{33}^R$  being respectively (3,3) component of  $f^R$  and  $g^R$ . We define the diagonalization of  $m_\ell$  as  $D_\ell \equiv V_{e_L}^{\dagger} m_\ell V_{e_R}$ .

<sup>&</sup>lt;sup>4</sup> Hereafter, we compute the loop diagrams with a method of mass insertion approximation. In particular, we do not perform diagonalization for new scalar particles.

#### C. Active neutrino mass matrix

The active neutrino mass is induced at one-loop level through interaction terms with couplings F and  $(H^{\dagger}\eta)^2$ , and given by [27]

$$(m_{\nu})_{ij} = \frac{(f_{33}^R)^2 M_0}{(4\pi)^2} \tilde{F}_{ia} \tilde{D}_{\alpha} \tilde{F}_{aj}^T \left[ \frac{\tilde{m}_R^2}{\tilde{m}_R^2 - \tilde{D}_{\alpha}^2} \ln \left[ \frac{\tilde{m}_R^2}{\tilde{D}_{\alpha}^2} \right] - \frac{\tilde{m}_I^2}{\tilde{m}_I^2 - \tilde{D}_{\alpha}^2} \ln \left[ \frac{\tilde{m}_I^2}{\tilde{D}_{\alpha}^2} \right] \right]$$
(17)

$$\equiv \kappa_{\nu}(\tilde{m}_{\nu})_{ij},\tag{18}$$

where  $\kappa_{\nu} \equiv (f_{33}^R)^2 M_0$ ,  $m_R \equiv M_0 \tilde{m}_R$  is the mass of  $\eta_R$  and  $m_I \equiv M_0 \tilde{m}_I$  is that of  $\eta_I$ . We define  $m_{\nu}$  is diagonalized by  $D_{\nu} = U_{\nu}^T m_{\nu} U_{\nu}$ . Then, the observed mixing matrix  $U \equiv V_{e_L}^{\dagger} U_{\nu}$  and  $\kappa_{\nu}$  can be rewritten in terms of rescaled neutrino mass eigenvalues  $\tilde{D}_{\nu} (\equiv D_{\nu}/\kappa_{\nu})$  and atmospheric neutrino mass-squared difference  $\Delta m_{\text{atm}}^2$  as follows:

(NH): 
$$\kappa_{\nu}^{2} = \frac{|\Delta m_{\text{atm}}^{2}|}{\tilde{D}_{\nu_{3}}^{2} - \tilde{D}_{\nu_{1}}^{2}}, \quad \text{(IH): } \kappa_{\nu}^{2} = \frac{|\Delta m_{\text{atm}}^{2}|}{\tilde{D}_{\nu_{2}}^{2} - \tilde{D}_{\nu_{3}}^{2}},$$
 (19)

where NH and IH respectively stand for the normal and inverted hierarchies, respectively. Subsequently, the solar neutrino mass-squared difference is determined by the relation

$$\Delta m_{\rm sol}^2 = \kappa_{\nu}^2 (\tilde{D}_{\nu_2}^2 - \tilde{D}_{\nu_1}^2). \tag{20}$$

The effective mass for neutrinoless double beta decay can be written by

$$\langle m_{ee} \rangle = \kappa_{\nu} | \tilde{D}_{\nu_{1}} \cos^{2} \theta_{12} \cos^{2} \theta_{13} + \tilde{D}_{\nu_{2}} \sin^{2} \theta_{12} \cos^{2} \theta_{13} e^{i\alpha_{2}} + \tilde{D}_{\nu_{3}} \sin^{2} \theta_{13} e^{i(\alpha_{3} - 2\delta_{CP})} |, \tag{21}$$

where  $\theta_{12,23,13}$  are mixing angles for U in the standard parametrization,  $\delta_{CP}$  is a Dirac CP phase, and  $\alpha_{2,3}$  are Majorana phases, defined in Majonara phase matrix P as  $P \equiv \text{diag}(1, e^{\alpha_2/2}, e^{\alpha_3/2})$ . A predicted value of  $\langle m_{ee} \rangle$  is constrained by the current KamLAND-Zen data;  $\langle m_{ee} \rangle < (28 - 122)$  meV at 90 % confidence level [33]. Furthermore the sum of neutrino masses is constrained by the minimal standard cosmological model  $\Lambda_{\text{CDM}} + \sum D_{\nu}$  that provides the upper bound  $\sum D_{\nu} \leq 120$  meV [34, 35], although it becomes weaker if the data are analyzed in the context of extended cosmological models [36]. Recently, DESI and CMB data combination provides more stringent upper bound on the sum as  $\sum D_{\nu} \leq 72$  meV [37]. Direct search for neutrino mass is done by the Karlsruhe Tritium Neutrino (KATRIN) experiment [38], which is the first sub-eV sensitivity on  $m_{\nu_e}^2 = (0.26 \pm 0.34) \text{ eV}^2$  at 90 % CL. Here,  $m_{\nu_e}^2$  is defined by

$$\kappa_{\nu}^{2} \left[ (\tilde{D}_{\nu_{1}} \cos \theta_{13} \cos \theta_{12})^{2} + (\tilde{D}_{\nu_{2}} \cos \theta_{13} \sin \theta_{12})^{2} + (\tilde{D}_{\nu_{3}} \sin \theta_{13})^{2} \right]. \tag{22}$$

In numerical analysis, we will adopt NuFit 6.0 [39] to experimental ranges of neutrino observables in addition to the above constraints of neutrino masses.

## D. LFVs, charged-lepton g-2 and EDMs

In this subsection, we will discuss LFVs, charged-lepton g-2 and EDMs, in order to compare with the experimental constraints in the numerical analyses. The dominant LFVs and charged-lepton g-2 and EDMs are induced via the following terms:

$$F'_{i\alpha}\overline{\ell_{L_i}}\psi_{R_\alpha}\eta^- + G'_{\alpha j}\overline{\psi_{R_\alpha}^C}\ell_{R_j}S^+ + \text{h.c.},$$
(23)

where  $F' \equiv V_{e_L}^{\dagger} F$ ,  $G' \equiv G V_{e_R}$ , and all the above partices are supposed to be mass eigenstates. Then, the branching ratios for LFVs, charged-lepton g-2 and EDMs are respectively given by

$$BR(\ell_i \to \ell_j \gamma) \approx \frac{48\pi^3 C_{ij} \alpha_{em}}{G_F^2 m_{\ell_i}^2} \left[ |a_{R_{ij}}|^2 + |a_{L_{ij}}|^2 \right], \tag{24}$$

$$\Delta a_{\ell_i} \approx -m_{\ell_i} \left[ a_{R_{ii}} + a_{L_{ii}} \right], \quad d_{\ell_i} = \frac{e}{2} \text{Im} \left[ a_{R_{ii}} - a_{L_{ii}} \right],$$
 (25)

where  $G_F$  is Fermi constant,  $\alpha_{\rm em} \approx 1/137$  is fine structure constant, and  $C_{21} \approx 1$ ,  $C_{31} \approx 0.1784$ ,  $C_{32} \approx 0.1736$ ,  $(\ell_1, \ell_2, \ell_3) \equiv (e, \mu, \tau)$ .  $a_R$  and  $a_L$  in our model are respectively computed as follows:

$$a_{R_{ij}} \approx \frac{\sqrt{2}v_H \mu_0'}{(4\pi)^2 M_0^3} \tilde{F}_{j\alpha}' \tilde{D}_{\alpha} \tilde{G}_{\alpha i}' F_{lfvs}, \quad a_{L_{ij}} \approx \frac{\sqrt{2}v_H \mu_0'}{(4\pi)^2 M_0^3} \tilde{G}_{j\alpha}'^{\dagger} \tilde{D}_{\alpha} \tilde{F}_{\alpha i}'^{\dagger} F_{lfvs}, \tag{26}$$

$$F_{lfvs} = \int dx_1 dx_2 dx_3 dx_4 x_5 \delta(1 - x_1 - x_2 - x_3 - x_4 - x_5) \left( \frac{3}{\Delta^2} + \frac{\tilde{m}_S^2 + \tilde{m}_\eta^2}{\Delta^3} \right), \tag{27}$$

where  $\Delta \equiv x_1 \tilde{D}_{\alpha}^2 + (x_2 + x_4) \tilde{m}_S^2 + (x_3 + x_5) \tilde{m}_{\eta}^2$  and  $x_i$ s are Feynman parameters.

Experimental upper bounds and future prospects for the branching ratios of the LFV decays are given by [40–43]

Current: BR(
$$\mu \to e\gamma$$
)  $\lesssim 3.1 \times 10^{-13}$ , BR( $\tau \to e\gamma$ )  $\lesssim 3.3 \times 10^{-8}$ , BR( $\tau \to \mu\gamma$ )  $\lesssim 4.4 \times 10^{-8}$ , (28)

Future: 
$$BR(\mu \to e\gamma) \lesssim 6.0 \times 10^{-14}$$
,  $BR(\tau \to e\gamma) \lesssim 9.0 \times 10^{-9}$ ,  $BR(\tau \to \mu\gamma) \lesssim 6.9 \times 10^{-9}$ . (29)

Experimental results for charged-lepton g-2 at  $1\sigma$  are given by [44–47]  $^5$ 

Current: 
$$\Delta a_e \simeq (3.41 \pm 1.64) \times 10^{-13}, \quad \Delta a_\mu \simeq (39 \pm 64) \times 10^{-11},$$
 (30)

Past: 
$$\Delta a_e \simeq (4.8 \pm 3.0) \times 10^{-13}$$
,  $\Delta a_\mu \simeq (25.1 \pm 5.9) \times 10^{-10}$  [49] or  $(24.9 \pm 4.8) \times 10^{-10}$  [50].

<sup>&</sup>lt;sup>5</sup> For  $\Delta a_e$ , there is another result by using the fine-structure constant  $\alpha$  determined by <sup>133</sup>C<sub>s</sub>, whose result has opposite sign,  $\Delta a_e = (-10.1 \pm 2.7) \times 10^{-13}$  [48].

Experimental upper bounds for EDMs are respectively given by [49]

$$|d_e| < 4.1 \times 10^{-30} \ e \text{ cm (JILA)}, \quad |d_{\mu}| < 1.9 \times 10^{-19} \ e \text{ cm (Muon g} - 2),$$
 (32)

$$|\text{Re}(d_{\tau})| < 4.5 \times 10^{-17} \ e \,\text{cm} \ (\text{Belle}), \quad |\text{Im}(d_{\tau})| < 2.5 \times 10^{-17} \ e \,\text{cm} \ (\text{Belle}).$$
 (33)

Furthermore, indirect bounds for the muon and tau EDMs provide more stringent constraints than the direct experimental ones, which are obtained by evaluating the muon-loop induced light-by-light CP odd amplitude [50, 51]:

$$|d_{\mu}| < 6.3 \times 10^{-21} \ e \,\text{cm}, \quad |d_{\tau}| < 4.1 \times 10^{-19} \ e \,\text{cm},$$
 (34)

by using the latest electron EDM bound. Note that these bounds are obtained by the current electron EDM bound, and therefore, an improvement of the electron EDM bound will also push down these upper bounds.

#### III. NUMERICAL RESULTS

Here, we perform  $\Delta \chi^2$  numerical analysis and investigate our allowed regions to satisfy whole the experimental results discussed above. Here, we assume all the relevant observables to be the Gaussian distribution under the  $\Delta \chi^2$  analysis, and hence,

$$\Delta \chi^2 = \sum_i \left( \frac{O_i^{\text{obs}} - O_i^{\text{th}}}{\delta O_i^{\text{exp}}} \right)^2, \tag{35}$$

where  $O_i^{\text{obs(th)}}$  is observed (theoretically obtained) value of corresponding observables and  $\delta O_i^{\text{exp}}$  indicates the experimental error at  $1\sigma$ . We adopt four reliable observables;  $\{\sin^2\theta_{12},\sin^2\theta_{13},\Delta m_{\text{atm}}^2,\Delta m_{\text{sol}}^2\}$ , to estimate the  $\Delta\chi^2$  analysis and take our allowed regions up to  $5\sigma^6$ . On the other hand, we independently request  $\sin^2\theta_{23}$  to be within  $3\sigma$  level of Nufit 6.0, since the experimental error is deviated from Gaussian distribution. In our parameter space, we fix  $f^R = f^L$  and  $g^R = g^L$  for simplicity  $^7$ . Then, we randomly select our input parameters as follows:

$$10^{-3} \le \frac{|\delta_{11,22,33}|}{\text{GeV}} \le 0.1, \quad 10^{-5} \le \frac{|\delta_{12,13,23}|}{\text{GeV}} \le 10^{-3}, \quad 10^{-5} \le \frac{|m_-|}{\text{GeV}} \le 0.1,$$
 (36)

$$10^{-7} \le \delta \tilde{m} \le 10^{-5}, \quad 10^{-5} \le |f_R| \le 1, \quad 10^{-5} \le |g_R| \le 0.1,$$
 (37)

$$100 \le \frac{M_0}{\text{GeV}} \le 10^5, \quad 0.1 \le \frac{\mu_0'}{\text{GeV}} \le 10, \quad 0.1 \le \tilde{m}_I \le 10, \quad 10^{-6} \le \tilde{m}_S \le 10^{-4},$$
 (38)

 $<sup>^{6}</sup>$  3 $\sigma$  with four degrees of freedom corresponds to  $\Delta\chi^{2} \approx 34.555$  [52].

<sup>&</sup>lt;sup>7</sup> Note that, this simplification does not eliminate all physical CP phases in our model: As mentioned in Eq. (4), we still have second example of the physical CP phase, as well as other ones which coming from, e.g., off-diagonal elements of  $f^{R(L)}$ ,  $g^{R(L)}$  and  $M_{R,L}$ . Therefore, we can discuss predictions for charged-lepton EDMs in our models.

| parameter             | BF                                   | parameter              | rameter BF                           |                           | BF                     |
|-----------------------|--------------------------------------|------------------------|--------------------------------------|---------------------------|------------------------|
| $s_{12}$              | 0.553                                | $s_{23}$               | 0.763                                | $s_{13}$                  | 0.147                  |
| $\Delta m_{ m sol}^2$ | $7.32 \times 10^{-23} \text{ GeV}^2$ | $\Delta m^2_{ m atm}$  | $2.54 \times 10^{-21} \text{ GeV}^2$ |                           |                        |
| $m_{ u_e}$            | $27.9~\mathrm{meV}$                  | $\sum D_{ u}$          | 111  meV                             | $D_{ u_1}$                | $26.5~\mathrm{meV}$    |
| $m_e$                 | 0.000511 GeV                         | $m_{\mu}$              | $0.106~{ m GeV}$                     | $m_{	au}$                 | 1.777 GeV              |
| $\Delta a_e$          | $8.74 \times 10^{-17}$               | $\Delta a_{\mu}$       | $2.52 \times 10^{-12}$               |                           |                        |
| $BR(\mu \to e\gamma)$ | $3.54 \times 10^{-24}$               | $BR(\tau \to e\gamma)$ | $2.35 \times 10^{-27}$               | $BR(\tau \to \mu \gamma)$ | $4.08 \times 10^{-21}$ |

TABLE II: Best-fit experimental values in the NH case, corresponding to  $\Delta \chi_{\rm min} \approx 1.06$ . Here we display these values that only depend on absolute values.

where  $\delta_{ij}$  is the component of  $m_+$ ,  $\tilde{m}_R \equiv \tilde{m}_I + \delta \tilde{m}$ ,  $\tilde{m}_\eta \equiv \tilde{m}_I$ . Arguments run over  $[-\pi, +\pi]$ . Note that arbitrary three components of  $g^R$  can directly be determined by charged-lepton mass matrix putting experimental results for charged-lepton masses. Here, we select  $g_{11,22,32}^R$ . Starting at the above regions in our input parameters, we specify the parameter space of their absolute values to fit the neutrino mass-square differences, three mixing angles, LFVs, and lepton g-2 9. But, we keep the wide ranges of their arguments that play a crucial role in determining the Dirac CP phase  $\delta_{CP}$ , two Majorana phases  $\alpha_{2,3}$  and EDMs  $d_{e,\mu,\tau}$ .

## A. NH

At first, we show our benchmark point that does not depend on phases in Table II. The best fit (BF) value corresponds to  $\Delta \chi_{\rm min} \approx 1.06$ . It is clear that the branching ratios for LFVs are enough small to satisfy current bounds. Moreover, the prediction of  $\Delta a_{\mu}$  is within  $1\sigma$  of current results, while that of  $\Delta a_e$  is within  $3\sigma$ .

Under Table II, we figure out the neutrinoless double beta decay in terms of phases  $\delta_{\rm CP}$ ,  $\alpha_2$ , and  $\alpha_3$  in Fig. 1, as blue, red and green points, respectively. The maximum value of neutrinoless double beta decay just reaches the upper limit of 28 meV. We find the following allowed region-tendencies of phases;  $30^{\circ} \lesssim \delta_{\rm CP} \lesssim 60^{\circ}$ ,  $200^{\circ} \lesssim \delta_{\rm CP} \lesssim 240^{\circ}$ ,  $-10^{\circ} \lesssim \alpha_2 \lesssim 0^{\circ}$  and  $-10^{\circ} \lesssim \alpha_3 \lesssim 20^{\circ}$ .

Next, we show our EDM predictions of  $|d_e|$  (left),  $|d_{\mu}|$  (center) and  $|d_{\tau}|$  (right) for the case of NH in Fig. 2, in term of three phases, where each of color plots are the same as the one in Fig. 1. These figures suggest that  $|d_e|$  reaches the experimental upper bound  $4.1 \times 10^{-30}$  e cm, while typical values

<sup>&</sup>lt;sup>8</sup> If there are no symbols of absolute values  $|\cdots|$  in Eqs. (36)-(38), such parameters are considered as real parameters.

<sup>&</sup>lt;sup>9</sup> This is because there are too many parameters and too much time to find out all the allowed regions.

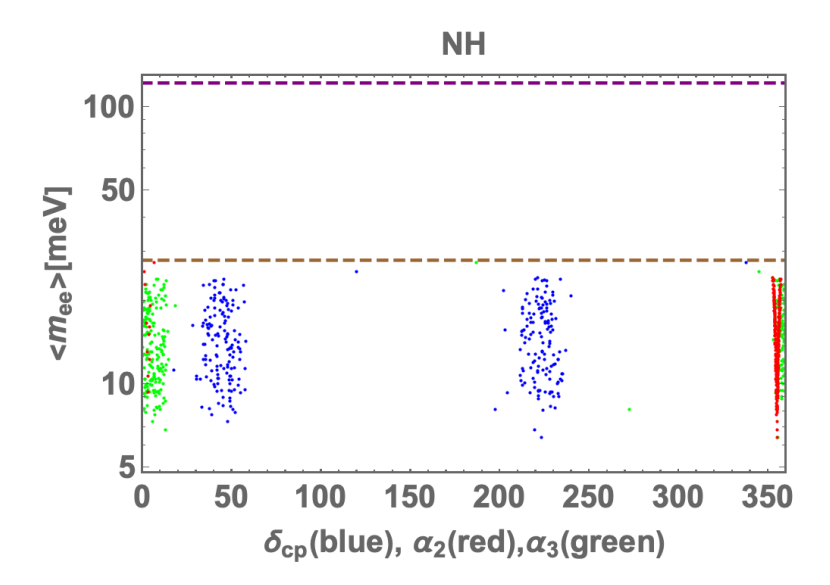


FIG. 1: Allowed regions for  $\langle m_{ee} \rangle$  in terms of phases  $\delta_{\rm CP}$  (blue),  $\alpha_2$  (red), and  $\alpha_3$  (green) in case of NH. Brown (lower) and purple (upper) dashed lines correspond to  $\langle m_{ee} \rangle = 28$  meV and 122 meV, respectively.

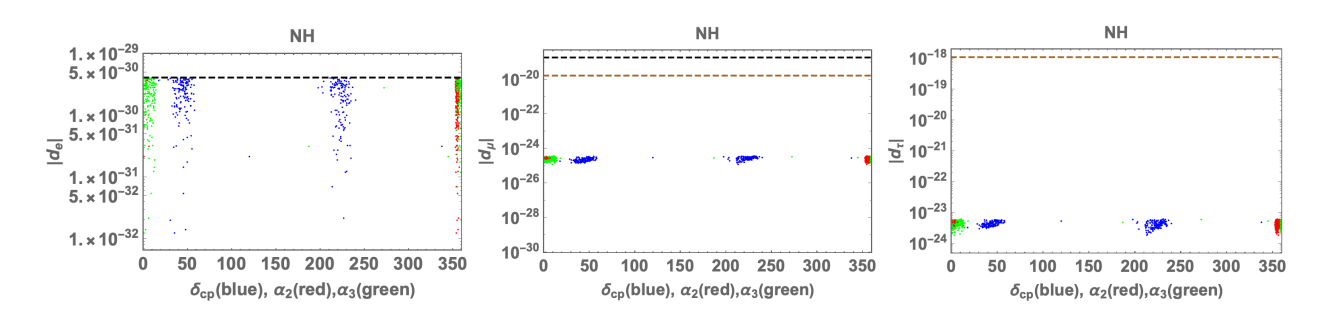


FIG. 2: Allowed regions for EDMs in terms of phases  $\delta_{CP}$ ,  $\alpha_2$ , and  $\alpha_3$  in case of NH, with same color manner as in Fig. 1. Black dashed line is the direct experimental upper bound, while brown one corresponds to the indirect upper bound.

of muon and tau EDM are  $|d_{\mu}| \simeq (1\text{-}4) \times 10^{-25}~e$  cm and  $|d_{\tau}| \simeq (2\text{-}6) \times 10^{-24}~e$  cm. Interestingly, the constraint  $|d_e| < 4.1 \times 10^{-30}~e$  cm results in  $\langle m_{ee} \rangle \lesssim 28$  meV, which is more stringent upper limit of the neutrinoless double beta decay. It is also emphasized that the predictions of  $|d_{\mu}|$  and  $|d_{\tau}|$  are several orders of magnitude larger than those from the minimal-flavor violation relation:  $|d_{\mu}| \simeq |d_e| (m_{\mu}/m_e) \lesssim 8.5 \times 10^{-28}~e$  cm and  $|d_{\tau}| \simeq |d_e| (m_{\tau}/m_e) \lesssim 1.4 \times 10^{-26}~e$  cm. This is because origins of physical CP phases for  $d_{e,\mu,\tau}$  are different from each other. Another interesting point is mostly fixed predictions of  $|d_{\mu}|$  and  $|d_{\tau}|$  are obtained by the focused benchmark point. This is because they tend to be determined by the arguments whose allowed region is narrow for our input

| parameter             | BF                                   | parameter              | BF                                   | parameter                 | BF                     |
|-----------------------|--------------------------------------|------------------------|--------------------------------------|---------------------------|------------------------|
| $s_{12}$              | 0.557                                | $s_{23}$               | 0.695                                | $s_{13}$                  | 0.150                  |
| $\Delta m_{ m sol}^2$ | $7.60 \times 10^{-23} \text{ GeV}^2$ | $\Delta m^2_{ m atm}$  | $2.47 \times 10^{-21} \text{ GeV}^2$ |                           |                        |
| $m_{ u_e}$            | $48.6~\mathrm{meV}$                  | $\sum D_{ u}$          | $98.6~\mathrm{meV}$                  | $D_{\nu_3}$               | $0.0166~\mathrm{meV}$  |
| $m_e$                 | $0.000511~{ m GeV}$                  | $m_{\mu}$              | $0.106~{ m GeV}$                     | $m_{	au}$                 | 1.777 GeV              |
| $\Delta a_e$          | $7.35 \times 10^{-16}$               | $\Delta a_{\mu}$       | $2.95 \times 10^{-11}$               |                           |                        |
| $BR(\mu \to e\gamma)$ | $3.93 \times 10^{-20}$               | $BR(\tau \to e\gamma)$ | $1.78 \times 10^{-23}$               | $BR(\tau \to \mu \gamma)$ | $2.64 \times 10^{-17}$ |

TABLE III: Best-fit experimental values in the IH case, corresponding to  $\Delta \chi_{\rm min} \approx 0.539$ . Here we select the above values that dominantly depends on absolute values.

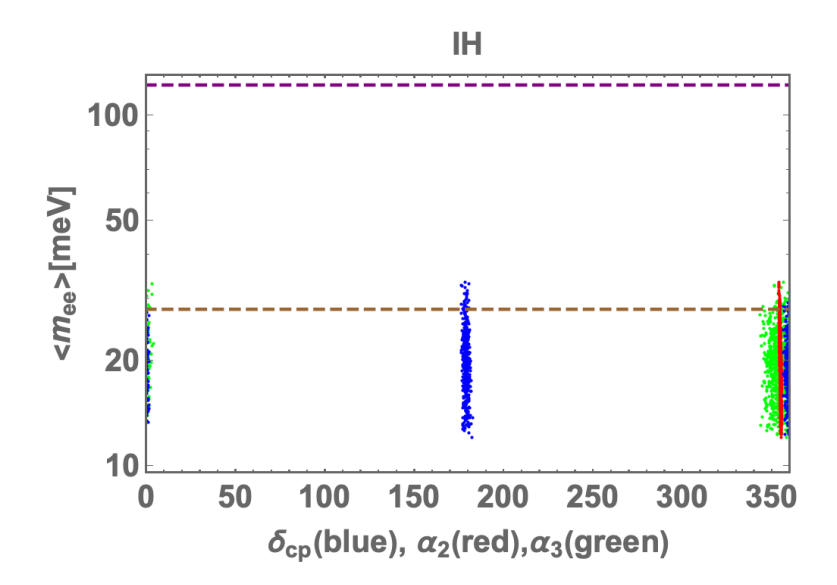


FIG. 3: Allowed regions for  $\langle m_{ee} \rangle$  in terms of phases  $\delta_{\text{CP}}$  (blue),  $\alpha_2$  (red), and  $\alpha_3$  (green) in case of IH. The meanings of dashed lines are same as in Fig. 1.

parameters, while  $|d_e|$  tends to be predicted by wide ones. <sup>10</sup>

#### B. IH

Next, we show our benchmark point that does not depend on phases in Table III. The BF value results in  $\Delta \chi_{\min} \approx 0.539$ . Compared with the case of NH, we obtain about one order of magnitude larger  $\Delta a_e$  and  $\Delta a_{\mu}$ . On the other hand, we found that the IH case predicts about four orders of

In fact, we found that some arguments are required to be narrow range for fitting the experimental observables, while some of them are not so strictly constrained. Although it might be interesting to explore its dependence, we will not show them in detail, since we have a lot of parameters. Note here that absolute values of  $d_{\mu}$  and  $d_{\tau}$  are much larger than those of  $d_{e}$ .

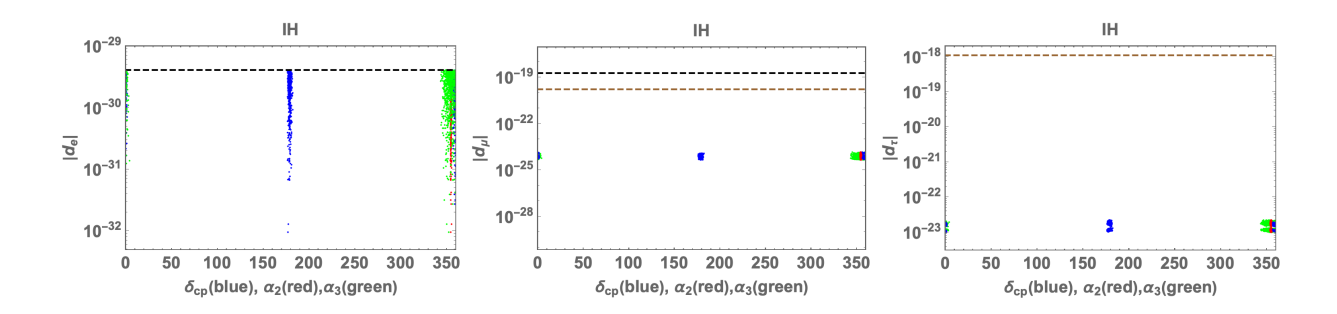


FIG. 4: Same plot as Fig. 2, but for the case of IH.

magnitude larger LFVs than those in the NH case, which still satisfy the current bounds.

Under Table III, we figure out the neutrinoless double beta decay in terms of phases  $\delta_{\rm CP}$ ,  $\alpha_2$ , and  $\alpha_3$  in Fig. 3, with same color manner as in Fig. 1. The several points exceed the upper limit of 28 meV, and the maximum value reaches 33.5 meV. We find  $\delta_{\rm CP}$  is localized at nearby 0° and 180°, while Majorana phases are  $\alpha_2 \sim 355^\circ$  and  $-20^\circ \lesssim \alpha_3 \lesssim 0^\circ$ .

In Fig. 4, we show EDMs  $|d_e|$  (left),  $|d_{\mu}|$  (center), and  $|d_{\tau}|$  (right), in term of three phases, where each of color plots are the same as the one in Fig. 1. These figures suggest that  $|d_e|$  can reach the experimental upper bound  $4.1 \times 10^{-30} \ e$  cm, but typical values of  $|d_{\mu,\tau}|$  are respectively  $10^{-24} \ e$  cm and  $10^{-23} \ e$  cm. Interestingly, the constraint  $|d_e| < 4.1 \times 10^{-30} \ e$  cm leads us to the similar result of the NH case;  $\langle m_{ee} \rangle \lesssim 33.5 \ meV$  which is just above the stringent upper limit of the neutrinoless double beta decay. The EDM dependencies are similar to those in the NH case.

#### IV. SUMMARY AND DISCUSSION

We have proposed a radiatively induced lepton mass model by introducing a  $Z_2$  gauging  $Z_5$  fusion rule to forbid tree level lepton masses while keeping relevant interactions to induce them via radiative corrections. The charged-lepton mass matrix is generated at one loop level via dynamical breaking of the fusion rule. On the other hand, the neutrino mass matrix is induced at one-loop level without breaking the fusion rule. These facts lead us to discuss LFVs, electron and muon g-2 and charged-lepton EDMs, where these phenomenology originate from the charged-lepton sector.

Due to too many free parameters, we have specified the absolute values of parameter set in order to fit the neutrino oscillation data and the charged-lepton mass observables. In addition, we have fixed the set of best fit values in cases of NH and IH. Then, once we have randomly selected the arguments of our free parameters and scanned whole their ranges, we have obtained our observables such as the Dirac CP phase, two Majorana phases, charged-lepton EDMs and the neutrinoless double beta decay, all of which depends on their arguments. As results of our numerical analyses, we have found several interesting tendencies;  $30^{\circ} \lesssim \delta_{\text{CP}} \lesssim 60^{\circ}$ ,  $200^{\circ} \lesssim \delta_{\text{CP}} \lesssim 240^{\circ}$ ,  $-10^{\circ} \lesssim \alpha_2 \lesssim 0^{\circ}$  and  $-10^{\circ} \lesssim \alpha_3 \lesssim 20^{\circ}$  in NH, and  $\delta_{\text{CP}} \sim 0^{\circ}$ ,  $180^{\circ}$ ,  $\alpha_2 \sim 355^{\circ}$  and  $-20^{\circ} \lesssim \alpha_3 \lesssim 0^{\circ}$  in IH. We have also discovered that the constraint  $|d_e| < 4.1 \times 10^{30}$  e cm has led us to the maximum prediction of  $\langle m_{ee} \rangle$  to be 28 meV for NH and 33.5 meV for IH, both of which are around more stringent upper limit of the neutrinoless double beta decay. Furthermore, the predictions of the muon and tau EDMs are several orders of magnitude larger than those obtained by the rough minimal-flavor violation relation, due to different origin of the CP phase.

Before closing our paper, we comment on a possible dark matter candidate in the model. Potentially, we have two dark matter candidates; the lightest neutral fermion  $\psi_{R_1}$  or the lightest neutral component of  $\eta$  which are similar to the case of the Ma model. However, our allowed mass region through the numerical analysis suggests that these masses are  $\mathcal{O}(1)$  PeV scale in case of  $m_S \sim 100$  GeV, and DMs decay so quickly that they cannot be DM candidates. In case of bosonic one, it decays into e.g., pairs of  $\bar{\ell}\ell$  through  $y^{\ell}$ . In case of fermionic one, it decays into  $\ell^-W^+\nu$  through  $g^{L/R}$  and kinetic term of  $\eta$  due to mixing between  $S^+$  and  $\eta^+$ . Thus, we concentrate on the other phenomenology in the current paper, instead of dark matter phenomenology. In a different parameter set, however, it would be a promising dark matter candidate which would be discussed in elsewhere.

## Acknowledgments

TN is supported by the Fundamental Research Funds for the Central Universities. HO is supported by Zhongyuan Talent (Talent Recruitment Series) Foreign Experts Project. YS is supported by Natural Science Foundation of China under grant No. W2433006.

<sup>[1]</sup> Z. Jiang, B.-Y. Qu, and G.-J. Ding (2025), 2510.07236.

<sup>[2]</sup> T. Kobayashi, H. Otsuka, M. Tanimoto, and T. T. Yanagida (2025), 2510.01680.

<sup>[3]</sup> S. Jangid and H. Okada (2025), 2508.16174.

<sup>[4]</sup> H. Okada and Y. Shigekami (2025), 2507.16198.

Y. Choi, H. T. Lam, and S.-H. Shao, Phys. Rev. Lett. 129, 161601 (2022), 2205.05086.

<sup>[6]</sup> C. Cordova, S. Hong, S. Koren, and K. Ohmori, Phys. Rev. X 14, 031033 (2024), 2211.07639.

<sup>[7]</sup> C. Cordova and K. Ohmori, Phys. Rev. X 13, 011034 (2023), 2205.06243.

- [8] C. Cordova, S. Hong, and S. Koren (2024), 2402.12453.
- [9] T. Kobayashi, H. Otsuka, and M. Tanimoto, JHEP 12, 117 (2024), 2409.05270.
- [10] T. Kobayashi and H. Otsuka, JHEP 11, 120 (2024), 2408.13984.
- [11] T. Kobayashi, Y. Nishioka, H. Otsuka, and M. Tanimoto, JHEP 05, 177 (2025), 2503.09966.
- [12] M. Suzuki and L.-X. Xu (2025), 2503.19964.
- [13] Q. Liang and T. T. Yanagida (2025), 2505.05142.
- [14] T. Kobayashi, H. Otsuka, M. Tanimoto, and H. Uchida (2025), 2505.07262.
- [15] T. Kobayashi, H. Mita, H. Otsuka, and R. Sakuma (2025), 2506.10241.
- [16] T. Kobayashi, H. Okada, and H. Otsuka (2025), 2505.14878.
- [17] T. Nomura and H. Okada (2025), 2506.16706.
- [18] J. Dong, T. Jeric, T. Kobayashi, R. Nishida, and H. Otsuka (2025), 2507.02375.
- [19] T. Nomura and O. Popov (2025), 2507.10299.
- [20] J. Chen, C.-Q. Geng, H. Okada, and J.-J. Wu (2025), 2507.11951.
- [21] T. Kobayashi, H. Otsuka, and T. T. Yanagida (2025), 2508.12287.
- [22] M. Suzuki, L.-X. Xu, and H. Y. Zhang (2025), 2508.14970.
- [23] G. Altarelli and F. Feruglio, Rev. Mod. Phys. 82, 2701 (2010), 1002.0211.
- [24] H. Ishimori, T. Kobayashi, H. Ohki, Y. Shimizu, H. Okada, and M. Tanimoto, Prog. Theor. Phys. Suppl. 183, 1 (2010), 1003.3552.
- [25] T. Kobayashi, H. Ohki, H. Okada, Y. Shimizu, and M. Tanimoto, <u>An Introduction to Non-Abelian Discrete Symmetries for Particle Physicists</u> (2022), ISBN 978-3-662-64678-6, 978-3-662-64679-3.
- [26] H. Ishimori, T. Kobayashi, H. Ohki, H. Okada, Y. Shimizu, and M. Tanimoto, An introduction to non-Abelian discrete symmetries for particle physicists, vol. 858 (2012).
- [27] E. Ma, Phys. Rev. D **73**, 077301 (2006), hep-ph/0601225.
- [28] K. S. Khaw, Y. Nakai, R. Sato, Y. Shigekami, and Z. Zhang, JHEP 02, 234 (2023), 2212.02891.
- [29] H. Okada and K. Yagyu, Phys. Rev. D 89, 053008 (2014), 1311.4360.
- [30] H. Okada and K. Yagyu, Phys. Rev. D **90**, 035019 (2014), 1405.2368.
- [31] M. E. Catano, R. Martinez, and F. Ochoa, Phys. Rev. D 86, 073015 (2012), 1206.1966.
- [32] Y. Kajiyama, H. Okada, and T. Toma, Eur. Phys. J. C 73, 2381 (2013), 1210.2305.
- [33] S. Abe et al. (KamLAND-Zen) (2024), 2406.11438.
- [34] S. Vagnozzi, E. Giusarma, O. Mena, K. Freese, M. Gerbino, S. Ho, and M. Lattanzi, Phys. Rev. D 96, 123503 (2017), 1701.08172.
- [35] N. Aghanim et al. (Planck), Astron. Astrophys. 641, A6 (2020), [Erratum: Astron. Astrophys. 652, C4 (2021)], 1807.06209.
- [36] K. A. Olive et al. (Particle Data Group), Chin. Phys. C 38, 090001 (2014).
- [37] A. G. Adame et al. (DESI) (2024), 2404.03002.
- [38] M. Aker et al. (KATRIN), Nature Phys. 18, 160 (2022), 2105.08533.

- [39] I. Esteban, M. C. Gonzalez-Garcia, M. Maltoni, I. Martinez-Soler, J. a. P. Pinheiro, and T. Schwetz, JHEP 12, 216 (2024), 2410.05380.
- [40] A. M. Baldini et al. (MEG), Eur. Phys. J. C 76, 434 (2016), 1605.05081.
- [41] B. Aubert et al. (BaBar), Phys. Rev. Lett. 104, 021802 (2010), 0908.2381.
- [42] F. Renga (MEG), Hyperfine Interact. 239, 58 (2018), 1811.05921.
- [43] K. Afanaciev et al. (MEG II), Eur. Phys. J. C 84, 216 (2024), [Erratum: Eur.Phys.J.C 84, 1042 (2024)], 2310.12614.
- [44] X. Fan, Ph.D. thesis, Harvard U. (2022).
- [45] X. Fan, T. G. Myers, B. A. D. Sukra, and G. Gabrielse, Phys. Rev. Lett. 130, 071801 (2023), 2209.13084.
- [46] S. Navas et al. (Particle Data Group), Phys. Rev. D 110, 030001 (2024).
- [47] L. Morel, Z. Yao, P. Cladé, and S. Guellati-Khélifa, Nature 588, 61 (2020).
- [48] R. H. Parker, C. Yu, W. Zhong, B. Estey, and H. Müller, Science 360, 191 (2018), 1812.04130.
- [49] A. Abada and T. Toma, JHEP 08, 128 (2024), 2405.01648.
- [50] Y. Ema, T. Gao, and M. Pospelov, Phys. Rev. Lett. 128, 131803 (2022), 2108.05398.
- [51] Y. Ema, T. Gao, and M. Pospelov, Phys. Lett. B 835, 137496 (2022), 2207.01679.
- [52] H. Okada and Y. Orikasa (2019), 1908.08409.